High-Index Faceted Ni₃S₂ Nanosheet Arrays as Highly Active and Ultrastable Electrocatalysts for Water Splitting

Liang-Liang Feng,[†,§] Guangtao Yu,[‡,§] Yuanyuan Wu,[†] Guo-Dong Li,[†] Hui Li,[‡] Yuanhui Sun,[‡] Tewodros Asefa,*[,#] Wei Chen,*[,‡] and Xiaoxin Zou*[,†]

[†]State Key Laboratory of Inorganic Synthesis and Preparative Chemistry, International Joint Research Laboratory of Nano-Micro Architecture Chemistry, College of Chemistry, Jilin University, Changchun 130012, P. R. China

[‡]Institute of Theoretical Chemistry, International Joint Research Laboratory of Nano-Micro Architecture Chemistry, Jilin University, Changchun 130023, P. R. China

[#]Department of Chemistry and Chemical Biology, and Department of Chemical and Biochemical Engineering, Rutgers, The State University of New Jersey, Piscataway, New Jersey 08854, United States

Ⓢ *Supporting Information*

ABSTRACT: Elaborate design of highly active and stable catalysts from Earth-abundant elements has great potential to produce materials that can replace the noble-metal-based catalysts commonly used in a range of useful (electro)chemical processes. Here we report, for the first time, a synthetic method that leads to *in situ* growth of {$\bar{2}10$} high-index faceted Ni₃S₂ nanosheet arrays on nickel foam (NF). We show that the resulting material, denoted Ni₃S₂/NF, can serve as a highly active, binder-free, bifunctional electrocatalyst for both the hydrogen evolution reaction (HER) and the oxygen evolution reaction (OER). Ni₃S₂/NF is found to give ~100% Faradaic yield toward both HER and OER and to show remarkable catalytic stability (for >200 h). Experimental results and theoretical calculations indicate that Ni₃S₂/NF's excellent catalytic activity is mainly due to the synergistic catalytic effects produced in it by its nanosheet arrays and exposed {$\bar{2}10$} high-index facets.

Production of hydrogen (H₂) via the water-splitting reaction in a sustainable way is one of the "holy grails" but remains an elusive goal in catalysis and renewable energy alike. This sustainability challenge has been unmet mainly because expensive noble-metal-based materials are still the best known catalysts to reduce the overpotentials of the two half-reactions involved in the water-splitting reaction: the hydrogen evolution reaction (HER) and the oxygen evolution reaction (OER).[1] Notably, Pt-based materials remain the most efficient electrocatalysts for HER, while Ir oxides remain the benchmark electrocatalysts for OER.[1,2] Due to the high cost and low Earth abundance of the metals in these catalysts, there is currently a dire need to develop alternative, inexpensive catalysts from Earth-abundant elements with good activity and durability for both half-reactions.

While there have been some reports on alternative, non-noble-metal-based electrocatalysts, the catalytic efficiency of many of them (e.g., MoS₂) is intrinsically limited by their low electrical conductivity, among other things.[1,3] Hence, the synthesis of non-noble-metal catalysts that possess metallic or conductive property deserves some special attention.[4] Ni₃S₂, a metal chalcogenide that occurs naturally as the mineral heazlewoodite, has intrinsic metallic behavior due to the presence of a continuous network of Ni—Ni bonds throughout its structure (see Theoretical Section in the Supporting Information (SI)). Besides its high conductivity, its low cost makes Ni₃S₂ quite suitable for various electrochemical applications.[5] While recently Ni₃S₂-based materials have been shown to be electrocatalytic active for either HER or OER,[6] their catalytic activity and stability are still less competitive than those of the noble-metal catalysts. It also remains unclear where exactly on the surfaces of the Ni₃S₂ the catalytic active sites promoting HER or OER occur, and a Ni₃S₂-based material that can catalyze both HER and OER efficiently has never been reported.

Beyond the motivation behind addressing these issues, it is also important to rationally design and synthesize the active sites of HER or OER catalysts to make their overall catalytic performance close to, or even better than, that of noble metals. While tailoring the size and assembly patterns of nanocatalysts can partially lead to this goal, increasing the density of the most catalytically active crystallographic facets on the surfaces of various nanomaterials is the most promising route to fully do so, as has recently been demonstrated for various noble metal and metal oxide catalysts.[7] In this context, high-index facets, denoted by a set of Miller indices {*hkl*} with at least one index larger than unity, can usually provide more catalytically favorable surface atomic structures (e.g., more atomic steps) than low-index facets. However, owing to their high surface energy, high-index facets are not stable, and they often evolve and disappear rapidly during the synthesis of the materials or their use in catalysis. Thus, making high-index faceted nanocatalysts with good structural stability is a challenging yet appealing conundrum to solve, toward meeting our goal of making efficient noble-metal-free (electro)catalysts.

Here we report, for the first time, the synthesis of stable, {$\bar{2}10$} high-index faceted Ni₃S₂ nanosheet arrays supported on nickel foam (NF), dubbed Ni₃S₂/NF. The material exhibits efficient and ultrastable electrocatalytic activity toward HER and OER,

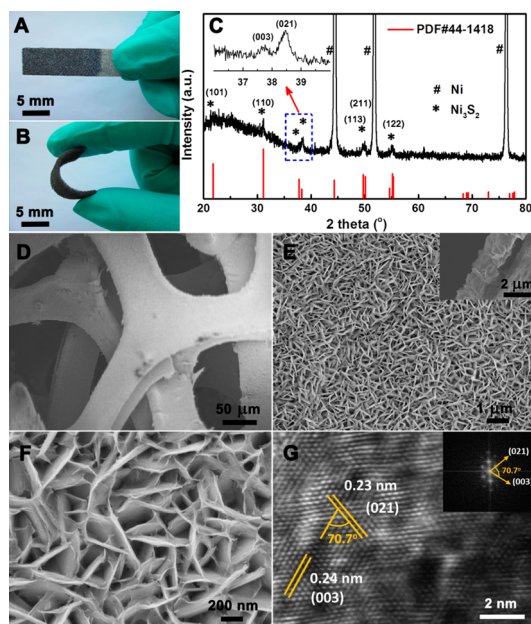**Figure 1.** (A,B) Digital images, (C) XRD pattern, and (D−F) top-view SEM images of the Ni_3S_2/NF. Inset in (E): side-view SEM image of Ni_3S_2/NF. (G) HRTEM image of the Ni_3S_2/NF, with the fast Fourier transform image shown in the inset.

Figure 2. (A) Steady-state current density as a function of applied voltage during HER at pH 7 over nickel foam (NF), Ni_3S_2 nanoparticles, Ni_3S_2/NF, and Pt/C (20 wt%). (B) Electrocatalytic efficiency of H_2 production over Ni_3S_2/NF (electrode area: 0.7 cm × 1 cm) at a current density of ca. 20 mA/cm², measured for 70 min. (C) Current density vs time ($I-t$) curve of HER over Ni_3S_2/NF at $\eta = 170$ mV over 200-h-long electrocatalytic HER. (D) Polarization curves obtained over Ni_3S_2/NF, before and after potential sweeps between 0 and −0.54 V for 10 000 cycles. Current density is normalized with the electrode's geometric surface area.

thanks to its advantageous nanocatalytic features as well as high-index facets. Theoretical calculations confirm that the $\{\overline{2}10\}$ high-index facets in Ni_3S_2/NF account for its uniquely efficient catalytic activity toward both HER and OER.

The Ni_3S_2/NF was synthesized by direct sulfidization of NF using thiourea, a source of sulfur, in a hydrothermal system at 150 °C for 5 h (see SI for further details). Figure 1A,B shows photographs of Ni_3S_2/NF before and after being stretched, indicating the material can be flexed well without undergoing structural damage. In addition, a strong adhesion between Ni_3S_2 and NF, whose amount is ~1.6 mg Ni_3S_2/cm² NF, is evidenced by the fact that the Ni_3S_2 nanosheets do not flake off of the material after 30 min of sonication. The powder XRD pattern of Ni_3S_2/NF shows that the material contains a hexagonal phase of Ni_3S_2 besides metallic nickel (Figure 1C). The formation of Ni_3S_2 is confirmed by Raman spectroscopy (Figure S1). The SEM images of Ni_3S_2/NF (Figure 1D−F) show that the 3D macroporous structure of NF remains intact in Ni_3S_2/NF (Figure 1D) and that the entire NF surface is homogeneously covered by the Ni_3S_2 nanosheets. Moreover, the Ni_3S_2 nanosheets appear to be vertically grown over the NF and spatially interconnected (Figure 1E,F), forming a lot of void spaces. The height of the Ni_3S_2 nanosheet array is ~2 μm (Figure 1E inset), and the thickness is 10−15 nm. In the HRTEM images of Ni_3S_2/NF (Figures 1G and S2), two sets of lattice fringes are observed, giving interplanar distances of 0.23 and 0.24 nm corresponding to the (021) and (003) crystallographic planes of hexagonal Ni_3S_2 phase. When the HRTEM image is obtained along the [100] crystallographic direction of Ni_3S_2, the observed angle between the (021) and (003) facets is 70.7°, very close to the theoretical value of 70.8°. This means the exposed facet of the nanosheets is $\{\overline{2}10\}$ (Figure S3). It is worth noting here that this facet has never before been realized experimentally for Ni_3S_2 materials. The presence of this facet is also confirmed by fast Fourier transform image (Figure 1G inset).
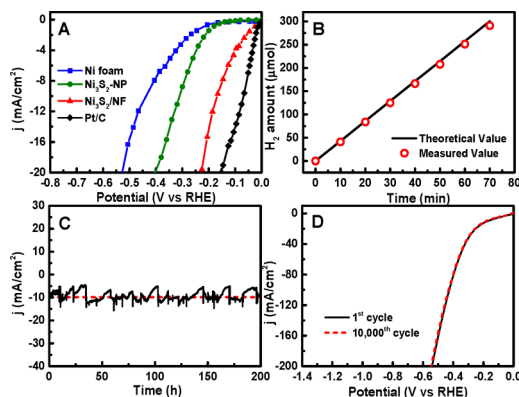
NF functions not only as a support material for the Ni_3S_2 nanosheets but also as a source of nickel during the *in situ* formation of the Ni_3S_2 nanosheets. When nickel nanoparticles (NPs), in lieu of NF, were used in the synthesis, only Ni_3S_2 NPs were obtained (Figure S4). This suggests NF is necessary for the synthesis of Ni_3S_2 nanosheet arrays, probably because NF promotes the unidirectional diffusion of nickel ions from its surface toward the solution. The amount of thiourea used in the reaction is also found to play a major role in the formation of Ni_3S_2/NF. When the amount of thiourea was halved, while keeping the other reaction parameters unchanged, Ni_3S_2 nanosheets did not form on the NF (Figure S5). On the other hand, when the amount of thiourea was increased 2- or 4-fold, the density of Ni_3S_2 nanosheets on NF decreased (Figure S6). Prolonging the reaction time led to a rapid increase in the thickness of Ni_3S_2 nanosheets and the appearance of {001} low-index facets (Figure S7) that ultimately dominated the exposed facets of the Ni_3S_2 nanosheets. This is not unexpected, because high-index facets often have high surface energy (see Theoretical Section in SI) and thus tend to evolve readily to more thermodynamically stable facets during crystal growth processes.

The electrocatalytic activity of Ni_3S_2/NF toward HER under neutral media (pH 7)[8] was evaluated using a typical three-electrode system, in which Ni_3S_2/NF was directly used as the working electrode (see SI for details). For comparison, the catalytic activity of NF, Ni_3S_2 NPs, and Pt/C (20 wt%) was also measured. Ni_3S_2/NF exhibits a remarkable catalytic activity toward HER (Figure 2A), much higher than that of Ni_3S_2 NPs. In fact, Ni_3S_2/NF produces a current density of 10 mA/cm² (the current density expected from a 12.3% efficient solar water-splitting device) at an overpotential (η) of ~170 mV, whereas Ni_3S_2 NPs give the same current density at a much higher η (310 mV). Ni_3S_2/NF's catalytic activity is also found to be better than that of most of the noble-metal-free HER catalysts reported for HER in neutral media (Table S1).

Figure 2B compares the amount of H_2 evolved experimentally versus the amount of H_2 theoretically expected in electro-chemical HER in the presence of Ni_3S_2/NF for 70 min. As can be seen in the graphs, Ni_3S_2/NF affords a stable H_2 evolution rate of
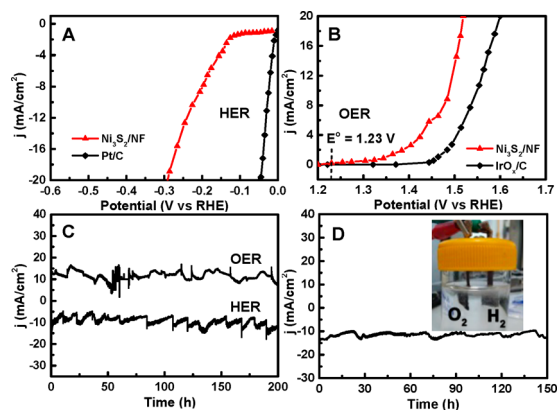
Figure 3. Steady-state current density as a function of applied voltage in alkaline media (pH 14) over Ni_3S_2/NF in (A) HER and (B) OER. (C) Current density vs time ($I-t$) curves of HER and OER with Ni_3S_2/NF recorded for over 200 h. (D) $I-t$ curve at pH 14 at an applied potential of 1.76 V for an electrolyzer whose anode and cathode both constitute Ni_3S_2/NF. Inset: a photograph showing generation of H_2 and O_2 bubbles on the Ni_3S_2/NF electrodes (see SI for a video). Current densities are normalized with the electrodes' geometric surface areas.

257.2 μmol/h, matching well with the amount expected theoretically. This reveals that Ni_3S_2/NF gives ∼100% Faradaic yield during HER in neutral medium.

To assess the stability of Ni_3S_2/NF, a current density vs time ($I-t$) curve was recorded over a longer reaction time (Figure 2C). The result shows that Ni_3S_2/NF retains its catalytic activity for at least 200 h. The total turnover number based on the moles of Ni in Ni_3S_2 after 200 h was found to be 1.87×10^3. The excellent stability of the material was further confirmed by the polarization curve obtained after 10 000 cycles, which was almost the same as the original one. After many such recycling tests, the morphology and microstructure of Ni_3S_2/NF were also intact, as evident from SEM and TEM images and X-ray photoelectron spectra (Figures S8 and S9).

Besides operating well as an electrocatalyst in neutral media for HER, Ni_3S_2/NF was also found to be a remarkably efficient electrocatalyst in basic media, and this time for both HER and OER. However, Ni_3S_2/NF is ineffective for HER in acidic media and for OER in acidic and neutral media (Figures S10 and S11). Ni_3S_2/NF affords a current density of 10 mA/cm^2 at small η = 223 and 260 mV for HER and OER, respectively, in basic solution (Figure 3A,B). Although the activity of Ni_3S_2/NF toward HER is lower than that of Pt/C (20 wt%), its activity toward OER is better than that of IrO_x (20 wt% IrO_x/C). Additionally, Ni_3S_2/NF shows ∼100% Faradaic yield (Figure S12) and excellent stability for >200 h for both HER and OER under basic media (Figures 3C and S13). It is also worth adding that Ni_3S_2/NF's stability for OER is much better than that of IrO_x. While Ni_3S_2/NF can retain its catalytic activity for over 200 h in OER (Figure 3C), IrO_x loses its activity by ∼60% after 15 h in OER (Figure S14). These results, coupled with its high activity and stability toward HER in neutral media, clearly demonstrate that Ni_3S_2/NF is a highly versatile, efficient electrocatalyst for both half-reactions involved in water splitting. Its activity and stability are also better than those of most of previously reported bifunctional electrocatalysts for water splitting (see Table S2).

Next, we assembled an electrolyzer whose anode and cathode both comprised Ni_3S_2/NF. When the applied voltage was set as ∼1.76 V, the electrolyzer gave a stable current density of ∼13 mA/cm^2 and retained that current density for at least 150 h
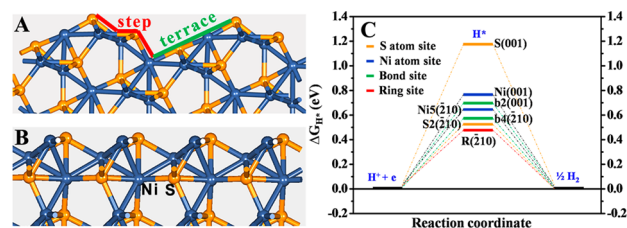

Figure 4. Most stable terminations of ($\bar{2}10$) (A) and (001) (B) surfaces of Ni_3S_2. (C) Calculated free-energy diagram of HER over ($\bar{2}10$) and (001) surfaces at equilibrium potential. The blue and yellow spheres represent Ni and S atoms, respectively, of Ni_3S_2.

(Figure 3D). The electrolyzer was also seen to generate large volumes of H_2 and O_2 gases on its respective Ni_3S_2/NF electrodes (see Figure 3D inset and SI video). This reveals that Ni_3S_2/NF has not only excellent stability but also a unique ability to serve effectively as electrocatalyst for both half-reactions of water splitting.

Ni_3S_2/NF's excellent catalytic performance can be accounted by the following four facts. (i) As Ni_3S_2 is intrinsically metallic, all the catalytically active sites on it are easily accessible to electrons coming from the electrode. (ii) The nanosheet array architecture provides Ni_3S_2/NF with a large active area, allowing more catalytic reactions to occur on it. This is corroborated by Ni_3S_2/NF's much higher electrochemical surface area than that of Ni_3S_2 NPs (Figure S15). (iii) Besides enhancing Ni_3S_2/NF's stability, the intimate contact between Ni_3S_2 nanosheets (the catalytically active phase) and NF (the support material) facilitates interfacial electron transport between the two. Rapid electron transfer in the presence of Ni_3S_2/NF is supported by electrochemical impedance spectroscopy (Figure S16), which shows the material has much lower Faradaic impedance than Ni_3S_2 NPs. (iv) Just like other high-index facets of other materials,[7] the {$\bar{2}10$} high-index facets of Ni_3S_2 have more favorable surface structure for catalysis than the low-index facets of Ni_3S_2, such as {001}. This is supported by the fact that the electrocatalytic activity toward HER and OER of the {$\bar{2}10$}-exposed Ni_3S_2/NF is higher than that of the {001}-exposed Ni_3S_2 nanosheet arrays (Figure S17).

To better understand the surface structures and the catalytic activity of high-index {$\bar{2}10$} and low-index {001} faceted Ni_3S_2, we performed density functional theory (DFT) computations by constructing the correlative theoretical models (Figures 4 and S18–S23). By comparing the computed surface energies of possible exposed terminations, we obtained ($\bar{2}10$) and (001) as the most energetically stable surfaces (the two are denoted as ($\bar{2}10$) and (001) in the following discussions and also SI, section 2.3). Unique atomic step-terraces on the ($\bar{2}10$) surface and the surface-ruffling (001) surface of Ni_3S_2 are observed (Figure 4A,B). This difference in structure also explains why the surface energy of the former (1.455 J/cm^2) is higher than that of the latter (1.054 J/cm^2).

Using DFT computations, the activity of the (001) surface toward HER was then evaluated. Some possible adsorption sites of H* are described in SI, section 2.4.1. Generally, the adsorption free energy of H* (ΔG(H*)) can serve as a good measure of the activity of a catalytic site toward HER (the smaller the ΔG(H*) absolute value of the site, the better its activity toward HER).[9] The Ni site is found to have a much smaller ΔG(H*) value (0.747 eV) than the S site (1.179 eV), indicating the former is more catalytically active (Figure S20). Additionally, this six-coordinated Ni atom can link to its neighboring seven-coordinated Ni atom and form Ni−Ni bonds (labeled by b2),

which can serve as the most active sites for HER on the (001) surface, with the smallest $\Delta G(H^*)$ value (0.693 eV) (Table S3). Thus, the Ni−Ni bonds and Ni sites are mainly responsible for the HER activity on the low-index (001) surface.

Next, the HER activity on the ($\overline{2}$10) surface was evaluated. Some possible adsorption sites of H* are described in SI, section 2.4.1. There are three types of S sites on the ($\overline{2}$10) surface, S1, S2, and S3, whose $\Delta G(H^*)$ values are 0.623, 0.520, and 1.018 eV, respectively (Figure S21, Table S3). All the S sites on the ($\overline{2}$10) surface are found to have smaller $\Delta G(H^*)$ values than those on the (001) surface (1.179 eV), indicating the HER activity is higher on the former (Figure 4C). This can be mainly due to the fact that the S sites (e.g., S1 and S2) on the ($\overline{2}$10) surface reside at the step edges and thus have a lower coordination number and a less crowded local environment.

Similarly, the degree of unsaturated coordination and the geometry around the two Ni sites (labeled by Ni4 and Ni5) on the ($\overline{2}$10) surface (Figure S21) can affect the catalytic activity of these sites in HER. The six-coordinated Ni5 atom at the terrace ($\Delta G(H^*)$ = 0.623 eV) can show better HER activity than the seven-coordinated Ni4 atom on the ($\overline{2}$10) surface ($\Delta G(H^*)$ = 1.030 eV) (Table S3). The Ni5 atom is also better than the parallel six-coordinated Ni atom on the (001) surface ($\Delta G(H^*)$ = 0.747 eV) because (i) the large plane of the terrace on the ($\overline{2}$10) surface can endow the Ni5 site with negligible steric effect and (ii) the Ni5 site is out-of-plane of the terrace more than the Ni site on the (001) surface is (Figure S22), making the former more easily accessible to reactants. This is further reflected by the fact that the Ni−Ni bond sites involving the Ni5 atoms on ($\overline{2}$10) surface, namely b4 (Ni5−Ni4, $\Delta G(H^*)$ = 0.542 eV) and b3 (Ni5−Ni3, $\Delta G(H^*)$ = 0.679 eV), exhibit better catalytic activity for HER than the other Ni−Ni bond sites without Ni5 atoms (b1 and b2), and even better than the Ni−Ni bond sites on the (001) surface (Table S3). Obviously, the ($\overline{2}$10) surface has more-active Ni and Ni−Ni sites than the (001) surface (Figure 4C). Particularly, there is one R ring site containing two Ni5 sites on the terrace of ($\overline{2}$10) surface (Figure S21) that can act as the most active site, due to its having the smallest $\Delta G(H^*)$ (0.496 eV). The high activity of the R ring site is due to its more functional moieties, involving two key Ni5 sites that interact better with reactants. Overall, owing to its unique step-terrace, the high-index ($\overline{2}$10) surface possesses more-active S- and Ni-related HER-active sites than the low-index (001) surface, quite consistent with our experimental results (Figure S17A).

After elucidating the HER activity of ($\overline{2}$10) surface, we analyzed the material's activity toward OER following the approach proposed by Nørskov et al. (SI, section 2.4.2).[10] Computed free-energy diagrams of OER and the correlative intermediates on the ($\overline{2}$10) and (001) surfaces are presented in Figure S23. All of the steps on the ($\overline{2}$10) and (001) surfaces were found to move uphill when no bias was applied (U = 0 V) (Figure S23, red lines). When the equilibrium potential (U = 1.23 V) for OER was applied, some steps moved downhill while others remained at uphill positions (Figure S23, blue lines). So, a bias must be applied on both surfaces to make every step of the energy diagram go downhill. The required overpotential values were 0.58 V for the ($\overline{2}$10) surface and 0.70 V for the (001) surface (Figure S23, black lines). This result indicates the ($\overline{2}$10) surface possesses better catalytic activity toward OER than does the (001) surface, in agreement with our experimental results (Figure S17B).

In conclusion, a bifunctional, binder-free, non-noble-metal electrocatalyst based on novel {$\overline{2}$10} facet-exposed Ni$_3$S$_2$ nanosheet arrays has been synthesized. The material is shown to efficiently catalyze both HER and OER. The material's excellent catalytic performance toward these reactions, which are relevant to water splitting, is attributed primarily to the synergistic effect between its nanosheet array architecture and {$\overline{2}$10} high-index facets. These properties as well as the durability and cost-effectiveness of Ni$_3$S$_2$/NF make it a promising material to replace noble-metal-based catalysts for water splitting.

■ ASSOCIATED CONTENT

Ⓢ Supporting Information

The Supporting Information is available free of charge on the ACS Publications website at DOI: 10.1021/jacs.5b08186.

> Video of electrocatalytic overall water splitting (AVI)
> Experimental details and supporting results (PDF)

■ AUTHOR INFORMATION

Corresponding Author

*tasefa@rci.rutgers.edu; xychwei@gmail.com; xxzou@jlu.edu.cn

Author Contributions

§L.-L.F. and G.Y. contributed equally.

Notes

The authors declare no competing financial interest.

■ ACKNOWLEDGMENTS

■ REFERENCES

(1) Zou, X.; Zhang, Y. *Chem. Soc. Rev.* **2015**, *44*, 5148.

(2) Zhao, Y.; Hernandez-Pagan, E. A.; Vargas, N. M.; Dysart, J. L.; Mallouk, T. E. *J. Phys. Chem. Lett.* **2011**, *2*, 402. Zou, X.; Goswami, A.; Asefa, T. *J. Am. Chem. Soc.* **2013**, *135*, 17242. McCrory, C. C. L.; Jung, S.; Ferrer, I. M.; Chatman, S. M.; Peters, J. C.; Jaramillo, T. F. *J. Am. Chem. Soc.* **2015**, *137*, 4347.

(3) Li, Y.; Wang, H.; Xie, L.; Liang, Y.; Hong, J.; Dai, H. *J. Am. Chem. Soc.* **2011**, *133*, 7296. Li, Y.; Hasin, P.; Wu, Y. *Adv. Mater.* **2010**, *22*, 1926.

(4) Examples: Faber, M. S.; Dziedzic, R.; Lukowski, M. A.; Kaiser, N. S.; Ding, Q.; Jin, S. *J. Am. Chem. Soc.* **2014**, *136*, 10053. Xu, K.; Chen, P.; Li, X.; Tong, Y.; Ding, H.; Wu, X.; Chu, W.; Peng, Z.; Wu, C.; Xie, Y. *J. Am. Chem. Soc.* **2015**, *137*, 4119. Wu, R.; Zhang, J.; Shi, Y.; Liu, D.; Zhang, B. *J. Am. Chem. Soc.* **2015**, *137*, 6983.

(5) Examples: Falkowski, J. M.; Concannon, N. M.; Yan, B.; Surendranath, Y. *J. Am. Chem. Soc.* **2015**, *137*, 7978. Zhou, W.; Zheng, J.-L.; Yue, Y.-H.; Guo, L. *Nano Energy* **2015**, *11*, 428.

(6) Jiang, N.; Bogoev, L.; Popova, M.; Gul, S.; Yano, J.; Sun, Y. *J. Mater. Chem. A* **2014**, *2*, 19407. Chung, D. Y.; Han, J. W.; Lim, D.; Jo, J.; Yoo, S. J.; Lee, H.; Sung, Y. *Nanoscale* **2015**, *7*, 5157. Zhou, W.; Wu, X.-J.; Cao, X.; Huang, X.; Tan, C.; Tian, J.; Liu, H.; Wang, J.; Zhang, H. *Energy Environ. Sci.* **2013**, *6*, 2921.

(7) Quan, Z.; Wang, Y.; Fang, J. *Acc. Chem. Res.* **2013**, *46*, 191. Liu, G.; Yang, H. G.; Pan, J.; Yang, Y. Q.; Lu, G. Q.; Cheng, H. *Chem. Rev.* **2014**, *114*, 9559.

(8) Sun, Y.; Liu, C.; Grauer, D. C.; Yano, J.; Long, J. R.; Yang, P.; Chang, C. J. *J. Am. Chem. Soc.* **2013**, *135*, 17699.

(9) Nørskov, J. K.; Bligaard, T.; Logadottir, A.; Kitchin, J. R.; Chen, J.; Pandelov, S.; Stimming, U. *J. Electrochem. Soc.* **2005**, *152*, J23. Liu, Y.; Yu, G.; Li, G.; Sun, Y.; Asefa, T.; Chen, W.; Zou, X. *Angew. Chem., Int. Ed.* **2015**, *54*, 10752.

(10) Valdés, Á.; Qu, Z.-W.; Kroes, G.-J.; Rossmeisl, J.; Nørskov, J. K. *J. Phys. Chem. C* **2008**, *112*, 9872.